In-situ force measurement during nano-indentation combined with Laue microdiffraction

Florian Lauraux, Sarah Yehya, Stéphane Labat, Jean-Sébastien Micha, Odile Robach, Oleg Kovalenko, Eugen Rabkin, Olivier Thomas, Thomas W. Cornelius

Received: 21 July 2020 | Revised: 23 September 2020 | Accepted: 9 October 2020

DOI: 10.1002/nano.202000073

RESEARCH ARTICLE

nano select WILEY

In-situ force measurement during nano-indentation combined with Laue microdiffraction

Florian Lauraux[1] | **Sarah Yehya**[1] | **Stéphane Labat**[1] | **Jean-Sébastien Micha**[2,3] | **Odile Robach**[2,3] | **Oleg Kovalenko**[4] | **Eugen Rabkin**[4] | **Olivier Thomas**[1] | **Thomas W. Cornelius**[1]

[1] Aix-Marseille Université, Université de Toulon, CNRS, IM2NP, Marseille, France

[2] CRG-IF BM32 Beamline at the European Synchrotron (ESRF), CS40220, Grenoble, France

[3] Institut de Recherche Interdisciplinaire de Grenoble (IRIG) CEA-IRIG, University of Grenoble Alpes, Grenoble, France

[4] Department of Materials Science and Engineering, Technion – Israel Institute of Technology, Haifa, Israel

Correspondence
Thomas W. Cornelius, Aix Marseille University, Université de Toulon, CNRS, IM2NP, Marseille, France.
Email: Thomas.Cornelius@im2np.fr

Funding information
Ministry of Science and Technology, Israel; Centre National de la Recherche Scientifique

Abstract

For the characterization of the mechanical properties of materials the precise measurements of stress-strain curves is indispensable. *In situ* nano-mechanical testing setups, however, may lack the precision either in terms of strain or stress determination. Recently, the custom-built scanning force microscope SFINX was developed which is compatible with third-generation synchrotron end-stations allowing for *in situ* nano-mechanical tests in combination with nanofocused synchrotron x-ray diffraction that is highly sensitive to strain and defects. The usage of a self-actuating and self-sensing cantilever tremendously increases the compactness of the system but lacks deflection sensitivity and, thus the force measurement. This deficiency is resolved by *in situ* monitoring the diffraction peaks of the Si cantilever by Laue microdiffraction during the nano-indentation of a gold crystal. The orientation and, hence, the deflection of the Si cantilever is deduced from the displacement of the Si Laue spots on the detector giving force accuracies of better than 90 nN. At the same time, the dislocation density in the indented Au crystal is tracked by monitoring the Au Laue spots eventually resulting in complete stress-dislocation density curves.

KEYWORDS
force measurement, in situ nano-indentation, Laue microdiffraction

1 | INTRODUCTION

In the recent past, the mechanical behavior of small scale materials attracted enormous attention. Pioneered by Uchic et al.[1,2] in the early 2000s, numerous micro-compression experiments were performed on metal and semiconductor micropillars revealing an increasing yield strength with decreasing structure size, a trend that became known in literature as "smaller is stronger."[3–8] While these microstructures were all prepared by focused ion beam (FIB) milling, Bei et al.[9,10] and Zimmermann et al.[11] reported that single-crystal Mo-alloy fibers obtained by selective etching of the Ni-Al matrix from the rod Mo-(NiAl) eutectics did not show any size effect in their as-grown state and exhibited yield strengths close to the theoretical limit of the material. However,

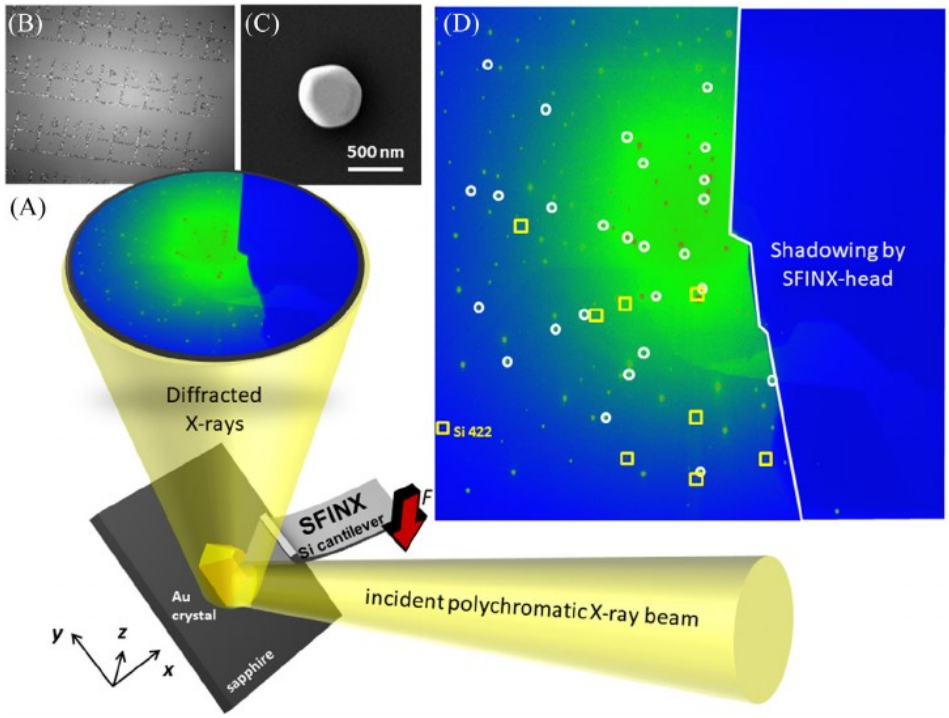

FIGURE 1 (A) Schematic representation of the experimental setup combining the custom-built atomic force microscope "SFINX" for nano-indentation and Laue microdiffraction. Scanning electron microscopy image (B) of the patterned array of Au crystals prepared by solid state dewetting on a *c*-oriented polished sapphire substrate and (C) of an individual Au crystal located in one of the 50 × 50 μm^2 squares shown in (B). D, Laue microdiffraction pattern of a gold crystal on a *c*-oriented sapphire substrate during nano-indentation. The Laue spots of the Au crystal and the Si tip used for nano-indentation are highlighted by white circles and yellow squares, respectively

pre-straining and FIB irradiation significantly reduced the yield strength by about one order of magnitude. Similar observations were reported for pristine Au nanoparticles obtained by solid state dewetting.[12] These findings raised the question about the influence of FIB milling on the actual state of the as-prepared microstructure regarding FIB-induced defects, surface amorphization, Ga^+ ion implantation in a surface near region, and side deposition of the milled material. They further clearly demonstrated the need for *in situ* nano-mechanical studies providing access to the actual microstructural state of the specimen during the whole deformation process. Since then, various *in situ* experimental setups in combination with scanning electron microscopy (SEM),[13,14] transmission electron microscopy (TEM),[15–17] and synchrotron x-ray diffraction techniques have been reported.[18–26]

Besides the observation of the sample deformation during mechanical loading, the measurement of the stress-strain curve is of paramount interest. Precise force measurements are particularly difficult to realize in crowded environments like in a TEM or at synchrotron beamlines. Atomic force microscopes (AFMs), that are compatible with third-generation synchrotron end-stations, have recently been developed. These AFMs are based on self-actuating and self-sensing AFM-probes (e.g., quartz tuning fork or Akiyama probe[27]) that significantly increase the compactness of the systems compared to a comparatively bulky standard laser feedback system.[18,28] While the synchrotron x-ray diffraction techniques such as Bragg coherent x-ray diffraction imaging and Laue microdiffraction provide direct access to the strain and defects in the nanostructure under study, the self-actuating and self-sensing AFM-probes lack deflection sensitivity and, thus a direct measure of the applied force.

Here, we demonstrate the *in situ* force measurement during nano-indentation of gold crystals on sapphire substrates using the custom-built AFM "SFINX" in combination with Laue microdiffraction (Figure 1A). The incident polychromatic x-ray beam not only illuminates the sample but also the Si tip of the self-actuating and self-sensing Akiyama-probe used in SFINX which eventually results in Laue diffraction signals of Au, sapphire, as well as of Si. From the displacement of the Si Laue diffraction pattern on the detector during nano-indentation the deflection of the Si cantilever is inferred allowing for determining the applied force *in situ* considering the stiffness of the cantilever as specified by the provider. The angular resolution of the rotation of the Si cantilever amounts to 5 millidegrees which translates to a force resolution of better than 90 nN. This *in situ* force measurement marks a major step

forward to actual *in situ* nano-mechanical studies on individual nanostructures in combination with synchrotron x-ray diffraction techniques facilitating the measurement of both stress and strain.

2 | EXPERIMENTAL METHOD

Gold crystals were prepared by solid state dewetting of a 30 nm gold thin film on a *c*-oriented polished sapphire substrate. The thin film was deposited by electron-beam evaporation on a lithographically patterned substrate which consisted of 2 μm large holes and a pitch of 50 μm. The sample was annealed in ambient air at 900°C for 24 hours which eventually resulted in individual Au crystals with a lateral size of ~500 nm and a height of ~300 nm located in the center of a 50 × 50 μm^2 large square. A SEM image of the patterned Au crystal sample on a sapphire substrate is presented in Figure 1B. The pattern consists of 20 rows indicated by letters each consisting of 20 squares numbered from 1 to 20. In each square an individual Au crystal like the one presented in Figure 1C can be found.

Laue microdiffraction was performed at the bending magnet beamline BM32 at the European Synchrotron ESRF in Grenoble (France). The polychromatic x-ray beam with an energy bandwidth from 5 to 25 keV was focused down to a size of 500 nm (H) × 500 nm (V) on the sample surface (which is inclined by 40° with respect to the incident beam) using a pair of Kirkpatrick-Baez mirrors. The diffracted x-rays were recorded by a sCMOS detector (*Photonic Science*) with 2018 × 2016 pixels and a pixel size of 73.4 μm × 73.4 μm which was installed at an angle of 90° with respect to the incident x-ray beam at a distance of 77 mm from the sample position. The recorded Laue microdiffraction patterns were indexed using the LaueTools software.[29]

For *in situ* nano-indentation experiments, which were performed under ambient conditions, the custom-built scanning force microscope "SFINX" was installed on the *x-y-z* translation stages of the conventional Laue microdiffraction setup as schematically illustrated in Figure 1A. The gold crystals were located by AFM topography imaging using SFINX and by x-ray fluorescence mapping of the Au L_{III} fluorescence yield employing a Röntec XFlash 1001 energy dispersive point detector. Once the SFINX-tip was positioned about 1 μm above the center of a selected gold crystal, the excitation of the Akiyama probe was stopped in order to avoid any fatigue-like effects while indenting the crystal using the SFINX silicon tip with a radius of curvature of 15 nm. The crystal was loaded with a constant speed of the vertical piezoelectric stage of 1 nm s^{-1}. After a holding time of 60 seconds, the crystal was then unloaded with a speed of 5 nm s^{-1}. During

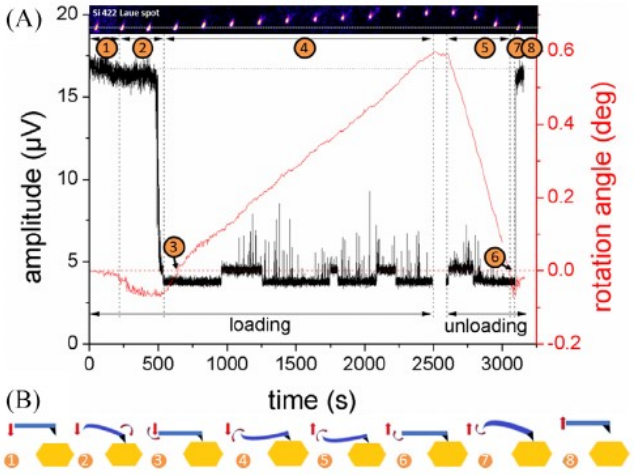

FIGURE 2 (A) Amplitude and rotation angle of the SFINX Si cantilever as a function of time. The inset shows a sequence of Laue microdiffraction patterns of the Si 422 Laue spot during loading-unloading of the Au crystal from which the rotation angle was inferred. There positions correspond to the moment in time at which they were recorded. (B) Schematic representations of the cantilever bending during loading and unloading of the Au crystal

the whole loading-unloading curve, Laue microdiffraction patterns were recorded simultaneously at a 0.25 Hz rate (exposure time of 3 seconds and readout time of about 1 second).

3 | RESULTS AND DISCUSSION

A Laue microdiffraction pattern of a gold crystal on a sapphire substrate with the SFINX-tip hovering about 1 μm above the crystal top facet is displayed in Figure 1D. Besides the expected Al_2O_3 Laue spots of the sapphire substrate and the Au Laue spots (highlighted by circles) of the gold crystal, another, less intense pattern of Laue spots (marked by squares) with a different crystalline symmetry is apparent. This latter Laue pattern can be indexed using Si as reference material. It actually originates from the Si tip of the Akiyama probe used in SFINX which is illuminated by the incident polychromatic x-ray beam and its tails.

When indenting the Au crystal with the SFINX Si-tip, the Si Laue spots move on the detector as illustrated by the sequence of Laue microdiffraction patterns of the Si 422 Laue spot (which is highlighted in Figure 1D) in the inset of Figure 2A. From the displacement of the Si Laue spots (the horizontal and vertical displacements of the Si 422 peak on the screen of the camera are exemplarily shown in Figure S1 in the supplementary material), the orientation of the Si cantilever was determined by indexing of the Si microdiffraction pattern and the calculation of the UB orientation matrix. This analysis shows that the cantilever rotates

exclusively in one plane (in the laboratory frame), bending downwards and upwards without any torsion.

The rotation angle of the Si cantilever and the approach-retract curve of the SFINX-tip as a function of time together with schematic representations of the SFINX-cantilever are presented in Figure 2A and B, respectively, and the different states of deflection of the cantilever are labelled accordingly. Despite the fact that the excitation of the cantilever was switched off prior to indentation, it oscillates with a very small amplitude resulting in an output voltage of the order of 17 μV at the pre-amplifier (compared to 1 V when the excitation is switched on) which is probably induced by environmental vibrations and noise (#1). When approaching the sample surface, the Si cantilever amplitude shows a slight progressive decrease and the rotation angle of the Si cantilever becomes negative reaching −0.067°, that is, it bends downwards towards the Au crystal (#2). As soon as the SFINX-tip touches the top facet of the Au crystal the oscillation is damped and the amplitude is further reduced to about 4 μV (#2). This transition from the free oscillation to a rigid contact with the gold crystal top surface takes about 100 seconds corresponding to an intermediate contact regime of about 100 nm (considering a constant speed of 1 nm s^{-1} of the piezoelectric stage). Once the SFINX-tip is in contact with the Au crystal, the downward bending of the Si cantilever is reduced, the cantilever passes through its horizontal position (#3) and then bends further and further upwards until the loading process is stopped (#4). The rotation angle of the SFINX Si-cantilever increases linearly with a slope of 3.4×10^{-4} deg s^{-1} reaching a maximum value of about 0.65°. As soon as the crystal is being unloaded (here with a speed of 5 nm s^{-1}), after a holding period of 1 minute, the rotation angle of the Si cantilever decreases again with a constant speed of 1.4×10^{-3} deg s^{-1} (#5). The cantilever crosses once more its horizontal position (#6) before being bent downward to −0.06° (#7). The cantilever then returns to its original horizontal position (#8). At the same time, the amplitude of the Si cantilever recovers its initial value of 17 μV signifying the free oscillation of the Si cantilever and the SFINX-tip being no longer in contact with the Au crystal. The downward bending of the cantilever just before regaining its free oscillation is caused by the sticking of the SFINX-tip on the Au crystal. During the complete loading-unloading process, while the SFINX-tip is in contact with the crystal, small fluctuations of the amplitude are apparent. These fluctuations may be caused by vibrations of the sample environment or photoelectric charging effects induced by the intense x-ray beam.

From the displacement of the Si Laue spots on the detector the actual bending angle of the Si cantilever was inferred. Considering the Si cantilever as a clamped beam with a force acting at its extremity, its deflection δ is calculated using the Euler-Bernoulli beam theory where F is the applied force, L is the beam length, E is the Young's modulus, and I is the second moment of the beam's cross-section.

$$\delta = \frac{FL^3}{3EI} \tag{1}$$

Here, we do not measure the deflection but the rotation angle α of the cantilever. Considering that the incident x-ray beam illuminates the Si tip and that the cantilever including tip is a single crystal, the rotation of the tip is the same as the cantilever at its extremity which is directly related to the bending and is given by the following equation[30]:

$$\alpha = \frac{FL^2}{2EI} \tag{2}$$

Substituting Equation (1) in Equation (2) results in the following expression that directly connects the rotation angle α with the deflection δ of the cantilever.

$$\delta = \frac{2}{3} L \cdot \alpha \tag{3}$$

Thus, considering the rotation angle α measured by Laue microdiffraction, the length of the cantilever of $L = 300$ μm as well as the cantilever stiffness of $k = 5$ N m^{-1} (as provided by NanoAndMore GmbH), the actually applied force is determined.

$$F = \delta \cdot k = \frac{2}{3} L \cdot \alpha \cdot k \tag{4}$$

The applied force as a function of the course of the vertical piezoelectric motor carrying the AFM-head is presented in Figure 3. The loading-unloading force-displacement curve shows the exact same features as the angular rotation of the SFINX Si cantilever. The downward bending is translated into a negative force due to the interaction of the SFINX Si-tip with the Au crystal. Once in contact, the applied force increases to up to 10.2 μN. A small kink is apparent at an applied force of about 2 μN which might originate from plasticity induced by the indentation. It should be noted that at this stage a major fraction of displacement z shown in Figure 3 corresponds to purely elastic bending of the Si cantilever, and only a small fraction of total displacement $z - \delta << z$ describes the penetration of the Si tip into the Au crystal. Finite element method simulations considering purely elastic contact between the Si tip and the Au particle indeed showed that the indentation depth for an applied force of 8 μN and a tip with a radius of curvature of 15 nm amounts to less than 10 nm (see Supplementary Material). During the unloading, the force decreases continuously, becomes negative due to

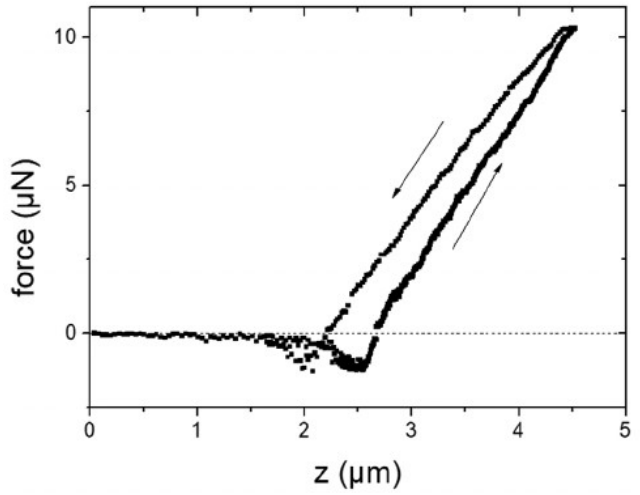

FIGURE 3 Applied force inferred from the rotation of the Si cantilever as a function of the displacement of the piezoelectric stage carrying the AFM-head

the sticking of the Si-tip on the Au crystal top facet before the Si-tip finally detaches from the nanostructure. The slopes of the loading and the unloading curve differ from each other amounting to 5.7 and -4.6 N m^{-1}, respectively. While in indentation experiments the unloading curve typically exhibits a steeper slope than the loading curve, it is the opposite in the present study. This discrepancy actually originates from the fact that the piezoelectric stage carrying the AFM-head used in the present work misses a closed feedback loop, which corrects for piezoelectric hysteresis of the stage. This shortcoming, however, is of minor importance thanks to the *in situ* monitoring of the actual deformation of the nanostructure by Laue microdiffraction (as it will be demonstrated further below) instead of using the load-displacement curve as in ordinary ex situ indentation. The force resolution in the present work is defined by the angular resolution of the rotation of the SFINX Si cantilever, which was inferred from the scattering of the displacement of the Laue spot during indentation presented in Figure S1 of the Supplementary Information and which amounts to about a quarter of a pixel of the camera corresponding to 5 millidegrees which translates to 87 nN.

From the loading-unloading curve, the adhesion force between the Si tip and the Au crystal can be inferred. Considering the distance of 100 nm over which the SFINX Si-tip is attracted by the Au crystal during the loading process, it cannot originate from short-range van der Waals forces or electrostatic forces. This apparent long-range adhesion force is probably caused by a contamination of the sample with a carbon layer that is deposited on top of the Au particle by the intense and highly focused x-ray beam. This carbon deposition may originate either from the cracking of hydrocarbons by photoelectrons emitted from the nano-object (as reported for Au nanowires,[31] for Ag/Au core-shell nanowires,[32] and for Au crystals similar to those studied in the present work)[33] or from residuals of the photoresist used for the lithographic patterning, which is carbonized by the x-ray beam.

The force required to separate the Si-tip adhered to the top flat facet of the Au particle is thus estimated from the unloading curve employing the Johnson-Kendall-Roberts (JKR) adhesion model,[34] which describes the adhesion forces between two spherical solids under the assumption of purely elastic (Hertzian) deformations in the contact zone. According to the JKR model, the force F_{sep} required to separate two adherent solids is

$$F_{sep} = -\frac{3}{2}\Delta\gamma \cdot \pi \cdot R \tag{5}$$

where $\Delta\gamma$ is the adhesion energy between SiO_2 (which is supposed to cover the Si tip) and Au, expressed as

$$\Delta\gamma = \gamma_{Au} + \gamma_{SiO} - \gamma_{Au-SiO} \tag{6}$$

with γ_{Au}, γ_{SiO}, and $\gamma_{Au\text{-}SiO}$ being the surface energies of Au and of SiO_2, and the energy of the Au-SiO_2 interface, respectively. In Equation(5), R is the effective radius of the two contacting spheres. In the case one of the contacting surfaces being flat, R is simply the radius of the second solid in the contact couple. In the present case, $R \approx 15$ nm is the radius of curvature of the Si-tip. Considering the values of surface and interface energies from ref. [35], the adhesion energy amounts to $\Delta\gamma \approx 0.41$ J m^{-2} resulting in a separation force of $F_{sep} \approx 30$ nN, which is by a factor of ~50 lower than the experimental value found in the present work (see Figure 3). The elevated experimental value may thus be caused by an increase of the contact area between the Si-tip and the Au crystal due to a nanometric plastic indent, by the carbon layer deposited in the course of the experiment, or by humidity. Below, we will provide independent evidence supporting the hypothesis that the applied forces were high enough to cause plastic deformation in the Au particle.

A sequence of Laue microdiffraction patterns of the Au 222 Laue spot recorded *in situ* during the indentation of the Au crystal is presented in the inset of Figure 4. While the initial Au Laue spot has a circular shape, it develops a streaking along the vertical direction during the nano-indentation which remains even after unloading. This streaking indicates rotational gradients within the probed volume. Considering the fact that the streaking remains even after complete unloading evidences plasticity and the storage of dislocations in the material.

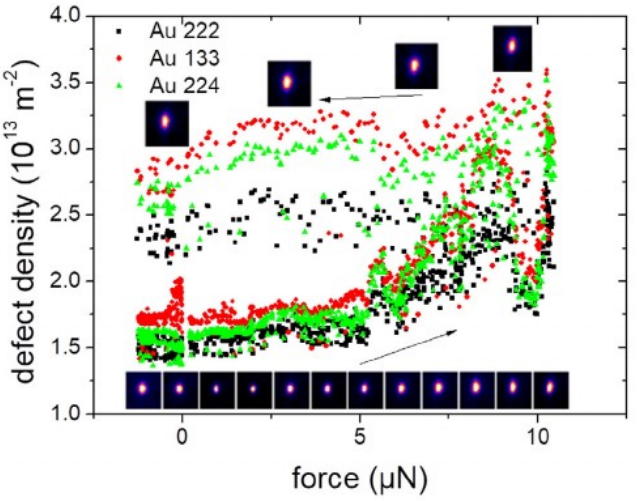

FIGURE 4 Dislocation density in the indented Au crystal as a function of the applied force inferred from the elongation of the Au 222, Au 133, and Au 224 Laue spot. The inset shows a sequence of Laue microdiffraction patterns of the Au 222 Laue spot recorded *in situ* during nano-indentation. There positions correspond to the force at which they were recorded

As suggested by Cahn[36] and Nye,[37] from the angular length θ of the peak broadening (obtained by the fitting of the peak shape using a Gaussian), the radius of curvature R of the crystal bending can be inferred, which allows for determining the density of geometrically necessary dislocations (GNDs) ρ that have to be stored in the crystal to accommodate such a change on the geometrical shape of the crystal:

$$\rho = \frac{1}{Rb} = \frac{\theta}{Lb} \tag{7}$$

Here, b is the Burger's vector and L is the length of the probed volume along b which is defined by the lateral crystal size of 500 nm in the present case. It should be noted that Equation (7) implies a homogeneous distribution of GNDs over the whole particle. This estimation takes into account GNDs and the activation of a single slip system while inhomogeneous strain fields induced by indentation are prone to activate several slip systems at the same time as well as to result in statistically stored dislocations (SSDs). Despite this strong simplification, the above estimation is expected to give the right order of magnitude of induced plasticity and dislocation density. Note that a dislocation density of the order of 10^{13} m^{-2} corresponds only to a few dislocations that are actually present in the small volume probed by the x-ray beam.

The GND density as a function of the applied force inferred from three different Laue spots (Au 222, 133, and 224) is presented in Figure 4 which all show the same behavior. At an applied force of about 2 μN the defect density starts increasing slightly and the increase becomes more pronounced for $F > 5$ μN. The defect density decreases significantly at $F \sim 10$ μN which might be caused by the exiting of dislocations from the Au crystal. The atomistic mechanisms of such dislocation egress to the side facets of the particle were described in refs. [38, 39] The defect density then increases again until the loading is interrupted. During the unloading the defect density reduces only to a minor degree illustrating that most of the dislocations generated towards the end of the indentation are stored within the crystal after complete unloading.

Besides the peak elongation, the Laue spot also slightly moves on the camera during nano-indentation. This displacement, which is reversible, indicates a rotation of the crystal of the order of few hundredth of a degree. The fact that the intensity of the Laue spot decreases in the very beginning of the indentation process may originate from a shadowing effect by the SFINX-tip.

In previous works, the force applied on nanostructures during *in situ* nano-mechanical tests could not be determined due to the absence of deflection sensitivity of the self-actuating and self-sensing AFM probe. The *in situ* deflection measurement of the Si cantilever and, thus direct force measurement during the nano-indentation of a gold crystal presented in this work marks a major step forward to obtain complete stress-strain information during nano-mechanical tests using the custom-built AFM "SFINX" in combination with Laue microdiffraction. It became feasible thanks to the CMOS-based diffraction detector whose noise is significantly lower than for CCDs used in previous studies, hence facilitating the detection of the very low intensity Si Laue spots originating from the SFINX Si-tip. Laue microdiffraction is highly sensitive to the crystal orientation providing accuracies of 5 millidegrees of the deflection of the Si cantilever which corresponds to a force resolution of 87 nN. This force resolution also applies to friction measurements where the cantilever is bent laterally. The current force resolution is at the limit of visualizing pop-ins and, thus the force-displacement curve presented in Figure 3 does not show the typical features expected during nano-indentation. It may, however, be further improved by using cameras with a smaller pixel size or installed in a larger distance from the sample, thus enhancing the angular resolution. The current upgrades of third-generation synchrotrons to extremely brilliant sources resulting in smaller source sizes with significantly lower beam divergence will lead to smaller focal spot sizes and higher flux densities which will enhance the visibility of the Si-tip Laue spots and will eventually allow for studying sub-100 nm nanostructures. Thus, the *in situ* force measurement with improved force resolution together with the new generation of synchrotron end-stations will enable us to obtain complete stress-strain information during

nano-mechanical testing of nanomaterials which are indispensable for the determination and understanding of the mechanical properties at the nanoscale, such as the nucleation of dislocations in defect scarce nanostructures and the release of ultra-high elastic stresses close to the theoretical yield strength of the material.

4 | CONCLUSION

In conclusion, the force applied during the nano-indentation of a gold crystal was measured *in situ* by monitoring the bending of the Si cantilever via the rotation of its Laue microdiffraction pattern. Simultaneously, the evolution of the Laue peak shape of the indented Au crystal was followed which provides direct access to the dislocation density in the nanostructure. Resolutions better than 90 nN were achieved, which can be further improved by the usage of detectors with smaller pixel sizes and being installed at larger distances, providing enhanced angular resolution of the rotation of the Si cantilever. This *in situ* force measurement is a major step forward to obtaining complete stress-strain information during *in situ* nano-mechanical testing in combination with synchrotron x-ray diffraction using custom-built AFMs that lack the deflection sensitivity of the Si cantilever due to spatial constraints at third-generation synchrotron beamlines with highly focused hard x-ray beams. By the insertion of a monochromator into a polychromatic x-ray beam a pre-defined x-ray energy can be selected, and thus the newly developed approach of measuring the applied forces can also be combined in the future with monochromatic and coherent x-ray diffraction.

ACKNOWLEDGMENTS

The authors gratefully acknowledge both the European Synchrotron Radiation Facility and the French CRG program committee for beamtime allocation at the BM32 beamline. They further thank the beamline staff for excellent support during the measurement campaign. The thin film processing was performed at the Micro-Nano Fabrication and PrintingUnit (MNF&PU), Technion. This research was partially supported by a grant from the Ministry of Science & Technology, Israel & France's Centre National de la Recherche Scientifique (CNRS).

ORCID

Thomas W. Cornelius https://orcid.org/0000-0003-4272-4720

REFERENCES

1. M. D. Uchic, D. M. Dimiduk, J. N. Florando, W. D. Nix, *Science* **2004**, *305*, 986.
2. M. D. Uchic, P. A. Shade, D. M. Dimiduk, *Annu. Rev. Mater. Res.* **2009**, *39*, 361.
3. J. R. Greer, W. C. Oliver, W. D. Nix, *Acta Mater.* **2005**, *53*, 1821. Erratum, Acta Mater. 2006, 54, 1705.
4. C. A. Volkert, E. T Lilleodden, *Philos. Mag.* **2006**, *86*, 5567
5. C. P. Frick, B. G. Clark, S. Orso, A. S. Schneider, E. Arzt, *Mater. Sci. Eng. A* **2008**, *489*, 319.
6. D. Kiener, C. Motz, T. Schoberl, M. Jenko, G. Dehm, *Adv. Eng. Mater.* **2006**, *8*, 1119.
7. F. Östlund, K. Rzepiejewska-Malyska, K. Leifer, L. M. Hale, Y. Tang, R. Ballarini, W. W. Gerberich, J. Michler, *Adv. Funct. Mater.* **2009**, *19*, 2439.
8. F. Östlund, P. R. Howie, R. Ghisleni, S. Korte, K. Leifer, W. J. Clegg, J. Michler, *Phil. Mag.* **2011**, *91*, 1190.
9. H. Bei, S. Shim, E. P. George, M. K. Miller, E. G. Herbert, G. M. Pharr, *Scripta Mater.* **2007**, *57*, 397.
10. H. Bei, S. Shim, G. M. Pharr, E. P. George, *Acta Mater.* **2008**, *56*, 4762.
11. J. Zimmermann, S. Van Petegem, H. Bei, D. Grolimund, E. P. George, H. Van Swygenhoven, *Scripta Mater.* **2010**, *62*, 746.
12. S. - W. Lee, D. Mordehai, E. Rabkin, W. D. Nix, *J. Mater. Res.* **2011**, *26*, 1653.
13. G. Richter, K. Hillerich, D. S. Gianola, R. Mönig, O. Kraft, C. A. Volkert, *Nano Lett.* **2009**, *9*, 3048.
14. D. Kiener, W. Grosinger, G. Dehm, R. Pippan, *Acta Mater.* **2008**, *56*, 580.
15. A. Minor, J. W. Morris Jr., E. A. Stach, *Appl. Phys. Lett.* **2001**, *79*, 1625.
16. J. Sun, L. He, Y.-C. Lo, T. Xu, H. Bi, L. Sun, Z. Zhang, S. X. Mao, J. Li, *Nat. Mater.* **2014**, *13*, 1007.
17. S. Lee, J. Im, Y. Yoo, E. Bitzek, D. Kiener, G. Richter, B. Kim, S. H. Oh, *Nat. Commun.* **2014**, *5*, 3033.
18. T. Scheler, M. Rodrigues, T. W. Cornelius, C. Mocuta, A. Malachias, R. Magalhães-Paniago, F. Comin, J. Chevrier, T. H. Metzger, *Appl. Phys. Lett.* **2009**, *94*, 023109.
19. C. Kirchlechner, J. Keckes, J. - S. Micha, G. Dehm, *Adv. Eng. Mater.* **2011**, *13*, 837.
20. R. Maaß, S. Van Petegem, H. Van Swygenhoven, P. M. Derlet, C. A. Volkert, D. Grolimund, *Phys. Rev. Lett.* **2007**, *99*, 145505.
21. H. Van Swygenhoven, S. Van Petegem, *JOM* **2010**, *62*, 36.
22. C. Leclere, T. W. Cornelius, Z. Ren, A. Davydok, J. - S. Micha, O. Robach, G. Richter, L. Belliard, O. Thomas, *J. Appl. Crystallogr.* **2015**, *48*, 291.
23. M. Dupraz, G. Beutier, T. W. Cornelius, G. Parry, Z. Ren, S. Labat, M.-I. Richard, G. A. Chahine, O. Kovalenko, E. Rabkin, M. Verdier, O. Thomas, *Nano Lett.* **2017**, *17*, 6696.
24. A. Davydok, T. W. Cornelius, Z. Ren, C. Leclere, G. Chahine, T. Schülli, F. Lauraux, G. Richter, O. Thomas, *Quantum Beam Sci.* **2018**, *2*, 24.
25. Z. Ren, T. W. Cornelius, C. Leclere, A. Davydok, J. - S. Micha, O. Robach, O. Ullrich, G. Richter, O. Thomas, *J. Appl. Phys.* **2018**, *124*, 185104.
26. T. W. Cornelius, O. Thomas, *Prog. Mater. Sci.* **2018**, *94*, 384.
27. T. Akiyama, U. Staufer, N. F. de Rooij, P. Frederix, A. Engel, *Rev. Sci. Instrum.* **2003**, *74*, 112.
28. Z. Ren, F. Mastropietro, S. Langlais, A. Davydok, M. - I. Richard, O. Thomas, M. Dupraz, M. Verdier, G. Beutier, P.

Boesecke, T. W. Cornelius, *J. Synchrotron Radiat*. **2014**, *21*, 1128.
29. J.-S. Micha, Lauetools: Open source Python packages for x-ray microlaue diffraction analysis, **2014**. https://gitlab.esrf.fr/micha/lauetools.
30. L. D. Landau, E. M. Lifshitz, *Theory of Elasticity (vol. 7 of Course of Theoretical Physics)*, 3rd ed. Elsevier, Amsterdam **1986**, p. 74.
31. J. Shin, T. W. Cornelius, S. Labat, F. Lauraux, M. I. Richard, G. Richter, N. P. Blanchard, D. S. Gianola, O. Thomas, *J. Appl. Crystallogr*. **2018**, *51*, 781.
32. S. T. Haag, M. I. Richard, U. Wetzel, V. Favre-Nicolin, O. Balmes, G. Richter, E. J. Mittemeijer, O. Thomas, *Nano Lett.* **2013**, *13*, 1883.
33. F. Lauraux, T. W. Cornelius, S. Labat, M. - I. Richard, S. Leake, T. Zhou, O. Kovalenko, E. Rabkin, T. U. Schülli, O. Thomas, *J. Appl. Crystallogr*. **2020**, *53*, 170.
34. K. L. Johnson, K. Kendall, A. D. Roberts, *Proc. R. Soc. Lond. A* **1971**, *324*, 301.
35. A. Kosinova, D. W, P. Schaaf, A. Sharma, L. Klinger, E. Rabkin, *Acta Mater.* **2018**, *149*, 154.
36. R. W. Cahn, *Proc. Phys. Soc.* **1950**, *63*, 323.
37. J. F. Nye, *Acta Metall.* **1953**, *1*, 153.
38. D. Mordehai, M. Kazakevich, D. J. Srolovitz, E. Rabkin, *Acta Mater.* **2011**, *59*, 2309.
39. O. Kovalenko, C. Brandl, L. Klinger, E. Rabkin, *Adv. Sci.* **2017**, *4*, 1700159.

SUPPORTING INFORMATION

Additional supporting information may be found online in the Supporting Information section at the end of the article.

How to cite this article: Lauraux F, Yehya S, Labat S, et al. In-situ force measurement during nano-indentation combined with Laue microdiffraction. *Nano Select*. 2020;1–8. https://doi.org/10.1002/nano.202000073